Available online at www.sciencedirect.com
ScienceDirect
Acta Materialia 56 (2008) 2262–2271
Acta MATERIALIA
www.elsevier.com/locate/actamat

Dislocation-climb plasticity: Modelling and comparison with the mechanical properties of icosahedral AlPdMn

F. Mompiou, D. Caillard *

CEMES-CNRS, 29 Rue Jeanne Marvig, BP 4347, 31055 Toulouse Cedex, France

Received 29 August 2007; received in revised form 10 January 2008; accepted 11 January 2008
Available online 5 March 2008

Abstract

A model of plasticity controlled by the pure climb motion of dislocations is proposed and compared with the mechanical properties of icosahedral AlPdMn. This model takes into account the chemical stress due to an out-of-equilibrium average concentration of vacancies, and the difficult nucleation of jog-pairs on climbing dislocations. It accounts for several unexplained properties of AlPdMn, namely a high strain-hardening at yield, a steady-state flow stress twice higher than the elastic limit, and two-stage relaxation curves. It also explains values of the stress–strain rate sensitivity larger than expected a priori, and activation energies larger than the self-diffusion one. The model may also be applicable to high-temperature deformation of crystals.

Keywords: Dislocations; Climb; Quasicrystals; Diffusion; Vacancies

1. Introduction

Although high-temperature creep by pure climb dislocation motion was proposed 40 years ago by Nabarro [1], this mechanism has, since then, never received much attention. One reason for this lack of interest is that plastic deformation is usually attributed to glide dislocation motion, climb being restricted to recovery.

There are, however, a few situations where climb has been shown to be the principal mode of plastic deformation. For instance, Le Hazif et al. [2] and Edelin and Poirier [3] showed that hexagonal-close-packed (hcp) magnesium and beryllium single crystals, strained along their *c*-axis, deform by the pure climb motion of c-dislocations. In a similar way, the high-temperature creep properties of intermetallic alloys and superalloys may also be controlled by pure climb, according to Epishin and Link [4] and Caillard [5].

As shown by Caillard and Martin [6], available models of climb are, however, insufficient to account for the experimentally measured mechanical properties, and corresponding activation parameters, for two main reasons: (i) the chemical force due to the lack or excess of vacancies, absorbed or emitted during deformation, is not taken into account, and (ii) usual low-stress approximations yielding a climb velocity proportional to effective stress are no more valid at high stress and/or large strain rates.

The aim of this study is thus to propose a reliable model of pure climb plasticity, including points (i) and (ii) above, which could be compared with the few available experimental data. Unfortunately, such a comparison is still impossible to make in crystals, where the total absence of glide is difficult to prove unambiguously, and where dislocation densities, chemical forces, internal stresses, and stress–strain rate dependences, have not all been determined. For this purpose, icosahedral AlPdMn, which deforms exclusively by dislocation climb [7–13], at least above 573 K, is a more convenient model material.

Dislocations and mechanical properties of quasicrystals have been reviewed recently in Ref. [14]. In spite of their specific aperiodic structures, these materials contain dislocations not significantly different from those in crystals [14–16]. In particular, dislocations have well-defined

* Corresponding author. Tel.: +33 5 62 25 78 72; fax: +33 5 62 25 79 99.
E-mail address: caillard@cemes.fr (D. Caillard).

1359-6454/$34.00
doi:10.1016/j.actamat.2008.01.015

Burgers vectors, which allow one to define unambiguous glide and climb mechanisms. In fact, the only difference between dislocations in quasicrystals and crystals is that the former trail phason walls (on account of the lack of periodicity) which, in contrast with stacking faults in crystals, can dissolve by a process called "retiling" or "phason dispersion". Under such conditions, most conclusions drawn from climb processes in quasicrystals can a priori be transposed to crystals.

The recent article of Ledig et al. [17], which provides the most complete set of experimental data on mechanical properties of AlPdMn, is used throughout this study. New results from in situ experiments are also presented to justify some important hypotheses.

2. The different components of stress

The deformation stress, σ, can be decomposed into the effective stress σ^*, which is involved in the expression of the dislocation-climb velocity, the chemical stress σ_{ch}, which results from over/under average concentrations of vacancies, the internal stress σ_i due to long-range elastic interactions between dislocations, and the phason stress σ_{ph} corresponding to the trailing of phason walls by moving dislocations. These different stresses are discussed and compared with measurements in the following sections. They are schematized at different steps of the stress–strain curve in Fig. 1.

2.1. The chemical stress, σ_{ch}

TEM observations in AlPdMn deformed in compression by Mompiou et al. [8] showed that many dislocations have moved by climb in planes almost perpendicular to the compression axis. These dislocations, denoted "1" in the scheme of Fig. 2, have the highest Schmid factor for climb (SF = 1). Contrast analyses of the phason walls trailed by these climbing dislocations showed that they absorb vacancies [8]. This results in a decrease of the average vacancy concentration, c, to below its original concentration at thermal equilibrium, $c_0 = \exp -\frac{U_{fv}}{kT}$. In this expression, U_{fv} is the formation energy of vacancies at free surfaces, or at dislocations. This builds a chemical (or osmotic) stress which can be expressed as [6]

$$\sigma_{ch} = \frac{kT}{\Omega} \ln \frac{c_0}{c}, \tag{1}$$

where Ω is the average atomic volume in the icosahedral structure. This stress opposes to the applied one, which results in a chemical strain-hardening $\theta_{ch} = \frac{\sigma_{ch}}{\varepsilon}$, where ε is the plastic deformation.

In pure climb compression, the amount of absorbed vacancies is proportional to the area swept by dislocations, which can be expressed by

$$\varepsilon = c_0 - c \tag{2}$$

The chemical hardening is accordingly:

$$\theta_{ch} = \frac{kT}{\Omega} \frac{\ln \frac{c_0}{c}}{c_0 - c}$$

Just above the elastic limit, where c remains close to c_0, it reduces to

$$\theta_{ch} = \frac{kT}{\Omega c_0} \tag{3}$$

This initial strain-hardening is higher than the elastic shear modulus, $\mu = 50$ GPa. For instance, it amounts to 118 GPa at 1000 K (with $c_0 = 7.5 \times 10^{-3}$ from Ref. [18] and $\Omega = 1.5 \times 10^{-29}$ m^3, from Ref. [19]), and to 323 GPa at 800 K (with $c_0 = 2.2 \times 10^{-3}$). Fig. 3 shows that these values are in a fair agreement with the initial strain-hardening measured by Ledig et al. [17], although these authors described it by the occurrence of an unknown stress, σ_{qc}. On the contrary, our conclusion is that the agreement between theoretical and experimental values of θ_{ch} confirms the

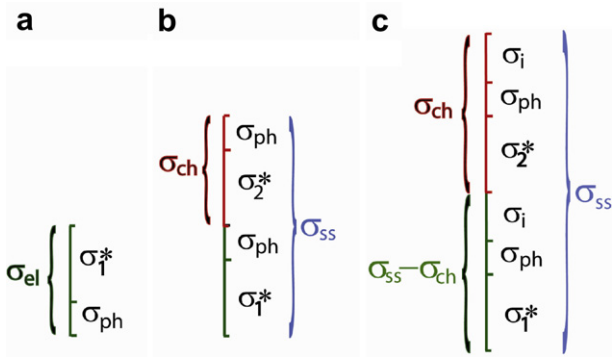

Fig. 1. Schematic description of the different components of stress at various stages of deformation: (a) elastic limit, (b) end of strain-hardening, (c) steady-state.

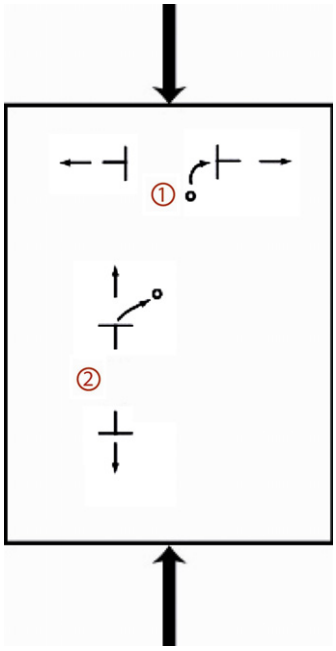

Fig. 2. Exchange of vacancies between dislocation families 1 and 2, under compression.

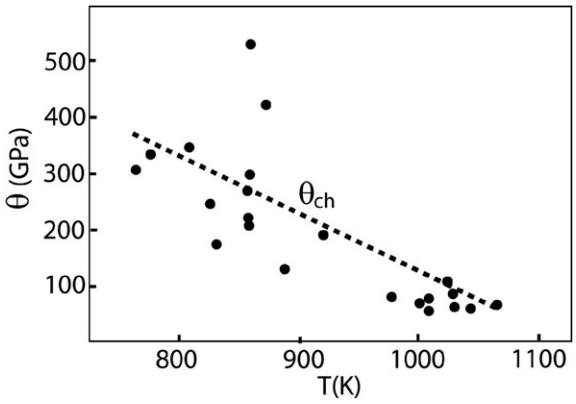

Fig. 3. Theoretical and experimental values of strain-hardening at yield. Experimental data are from Ledig et al. [17].

existence of the chemical stress expected in a climb-controlled plasticity mechanism.

The same TEM observations [8], confirmed by Ref. [20], also showed that many dislocations have moved by pure climb in planes parallel to the compression axis. These dislocations, noted "2" in the scheme of Fig. 2, have a zero Schmid factor for this kind of motion. They have accordingly moved and multiplied under a different kind of stress, which can be identified with the chemical force defined above. Contrast analyses confirmed that they emit vacancies [8], thus tending to compensate for the increase of the chemical stress, and to decrease accordingly the chemical hardening rate, θ_{ch}. Eventually, θ_{ch} decreases to zero when a steady-state is reached, for which all vacancies absorbed by the first system are provided by the second one. This occurs when

$$\rho_1 b_1 v_1 = \rho_2 b_2 v_2 \tag{4}$$

where indexes 1 and 2 refer to dislocation families moving at the respective velocities $v_1(\sigma - \sigma_{ch})$, and $v_2(\sigma_{ch})$ (Fig. 2). The Burgers vector lengths b_1 and b_2 are average values of several possible components of six-dimensional Burgers vectors in the physical space, which play the same role as usual Burgers vectors in crystals [21]. They can be considered to be equal (see Appendix). Dislocation densities are the result of a balance between multiplication and annihilation processes, which depend on the kinetics of motion under effective and internal stresses, respectively. We show in the Appendix that provided Eq. (4) is verified, the dislocation densities of the two systems evolve towards the steady-state values $\rho_{ss1} \approx \rho_{ss2}$. Then, Eq. (4) yields $v_1 \approx v_2$, which is realized for $\sigma - \sigma_{ch} \approx \sigma_{ch}$, namely:

$$\sigma_{ch} \approx \sigma_{ss}/2 \tag{5}$$

The stress–strain curve at low deformation, where internal stresses can be safely neglected, can thus be described as follows (Fig. 1a and b). The elastic limit, which corresponds to the first movements of "family 1" dislocations, is

$$\sigma_{el} = \sigma_1^* + \sigma_{ph} \tag{6}$$

where σ_1^* is the corresponding effective climb stress. After the rapid strain-hardening discussed above, the stress reaches a steady-state value σ_{ss}, which, according to Eqs. (5) and (6), and Fig. 1b, can be expressed as

$$\sigma_{ss} = \sigma_{el} + \sigma_{ch} = 2\sigma_{el} \quad \text{or} \quad \sigma_{ss} = 2(\sigma_1^* + \sigma_{ph}) \tag{7}$$

This equation shows that as soon as the equilibrium between emission and absorption of vacancies is attained, the steady-state stress is expected to be twice the elastic limit. The steady-state stress subsequently decreases according to the strain-softening mechanism specific of quasicrystals, which will be discussed in Section 2.2.

As predicted by the model, the elastic limit and the steady-state stress measured by Ledig et al. [17] are in a ratio of two, between 500 °C and 700 °C (Fig. 4). This property is difficult to check at higher temperatures, the accuracy of the measurements being insufficient above 700 °C. It is, however, clearly verified in the experiments of Brunner et al. [22], performed at 762 °C and 1% deformation, according to their Fig. 1 ($\sigma_{el} \approx 150$–200 MPa and $\sigma_{ss} \approx 340$ MPa). These results again confirm the validity of the dislocation-climb model.

It must be noted that the chemical stress is fundamentally different from the classical internal stress due to the elastic interaction between dislocations, although they both appear as a result of strain. In particular, the chemical stress can recover fairly rapidly upon unloading, as the vacancy concentration recovers its thermal equilibrium value, through the forward and backward motions of "family 2" and "family 1" dislocations, respectively. After subsequent reloading, the same elastic limit σ_{el} (increased by the permanent component σ_i), followed by the same strain-hardening θ_{ch}, must be anew observed. In that sense, the real permanent flow stress is $\sigma_{ss}/2$, instead of σ_{ss}. Geyer et al. [23] mentioned that a new elastic limit (called bump in their paper) actually occurs on re-loading after a stress relaxation test.

2.2. The effective climb stress σ^*

The dislocation-climb velocity is often considered to be $v = \frac{D_{sd}^{(v)}}{b}\frac{\Omega\sigma^*}{kT}$, where $D_{sd}^{(v)}$ is the vacancy self-diffusion

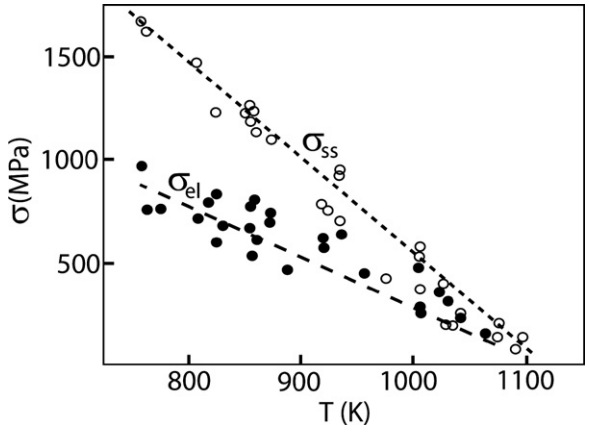

Fig. 4. Elastic limit and steady-state flow stress as a function of temperature, from Ledig et al. [17]. Note the ratio of 2 between the two types of stress.

coefficient ($D_{sd}^{(v)} = a^2 v_D \exp -\frac{U_{sd}^{(v)}}{kT}$), v_D is Debye frequency, a is the average interatomic distance, $U_{sd}^{(v)}$ is the self-diffusion energy of vacancies, b is the Burgers vector, and σ^* is the effective stress acting on climbing dislocations. However, this expression is valid only under very restrictive conditions, i.e. a very high jog density on climbing dislocations, and a low stress [6].

When the stress is high, and/or when the dislocation velocity is high, the jog density is determined by the rate of jog-pair nucleation on straight dislocation segments parallel to dense atomic rows. This behavior is supported by the observation of polygonal dislocations with edges parallel to twofold and pseudo-twofold directions, moving viscously in planes perpendicular to their Burgers vectors (see Ref. [11] and Fig. 5). The velocity of climb is then given by the model of Hirth and Lothe, originally derived for dislocation glide in semiconductors [6,12,24–26].

This model describes the nucleation and the extension of a jog/kink pair along a straight dislocation, with the assumption that jog/kink motion can be described by a diffusion equation. The threshold position, for which the attraction between opposite jogs is balanced by the effective stress, σ^*, is not attained in a single thermally activated event. This would indeed require the simultaneous diffusion of the N vacancies included in the jog-pair, with the high activation energy $NU_{sd}^{(v)} + U_{jp}^{(c)}(\sigma^*)$, where $U_{jp}^{(c)}(\sigma^*)$ is the threshold energy of an expanding jog-pair under the effective stress σ^*. On the contrary, the threshold position is attained after a series of elementary diffusion processes. Among the first-created jog-pairs separated by a single vacancy, a few ones evolve to a wider configuration embedding two vacancies, and so on, till a very few ones reach the critical position embedding N vacancies. According to this theory, the climb velocity can take two different forms (L being the length of a straight dislocation segment):

$$v = 2\pi a v_D \frac{\Omega\sigma^*}{kT} \exp -\frac{U_{sd}^{(v)} + \frac{1}{2}U_{jp}^{(c)}(\sigma^*)}{kT} \quad (8a)$$

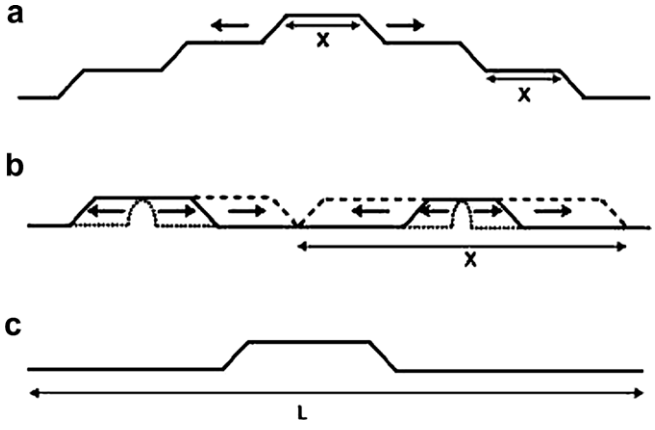

Fig. 5. The different regimes of climb controlled by nucleation and propagation of jog-pairs: (a) $X \ll L$, (b) $X \leqslant L$, and (c) $X \gg L$.

for $L > X$, in the so-called jog-collision regime, and

$$v = 2\pi L v_D \frac{\Omega\sigma^*}{kT} \exp -\frac{U_{sd}^{(v)} + U_{jp}^{(c)}(\sigma^*)}{kT} \quad (8b)$$

for $L < X$, in the so-called length-dependent regime where $v \propto L$.

The transition length X is the mean-free path of a jog issued from a jog-pair nucleation,

$$X = a \exp \frac{U_{jp}^{(c)}(\sigma^*)}{2kT}$$

Moving dislocations are curved in the first case (Fig. 5a), and straight along dense atomic rows in the second one (Fig. 5c). In metals, the jog-height h is the distance between adjacent dense atomic rows. The jog-height can, however, be larger in complex crystals with large cell sizes, where the dislocation core energy can vary with a periodicity larger than the interatomic distance. The same remark holds true for quasicrystals, where the dislocation energy can reach minimum values in Peierls valleys which are separated by various distances in the ratio of τ, the golden mean. The jog-height h is then the average distance between the deepest valleys.

Whether the dislocation-climb velocity is given by Eqs. (8a) or (8b) can be determined in in situ experiments (see Ref. [11] for a complete description of the method). Fig. 6a shows a polygonal dislocation with edges d_1 and d_2 parallel to twofold directions, moving by pure climb in a fivefold plane, at 740 °C. The straight aspect of dislocation segments seems to indicate that they move according to the length-dependent regime (Fig. 5c). However, Fig. 6b shows that there is no proportionality law between instantaneous velocities and dislocation lengths, in contrast with similar measurements in semi-conductors [6]. Dislocations accordingly move in the jog-collision regime, but close to the transition to the length-dependent one ($X \leqslant L$, Fig. 5b). More complete in situ experiments of the same kind can be found in Ref. [27].

When the temperature decreases, and since the apparent activation energy $U_{sd} + \frac{1}{2}U_{jp}(\sigma^*)$ must vary more or less proportionally to temperature, to keep a constant dislocation velocity (proportionality coefficient ck), the term $U_{jp}(\sigma^*) = 2(ckT - U_{sd})$ must decrease, and so must the mean-free path of jogs, X. This can account for the more curly dislocation shapes observed after low-temperature deformation.

At least below 800 °C, the stress dependence of the dislocation climb velocity is thus:

$$m = \frac{\partial \ln v}{\partial \ln \sigma^*} = 1 + \frac{\sigma^*}{2kT} \frac{\partial U_{jp}^{(c)}(\sigma^*)}{\partial \sigma^*} \quad (9)$$

which considering that jogs interact elastically at their threshold position [6], can be expressed as

$$m = 1 + \frac{1}{4\sqrt{2\pi}} \frac{\mu b^3}{kT} \sqrt{\frac{\sigma^*}{\mu}} \left(\frac{h}{b}\right)^{3/2} \quad (10)$$

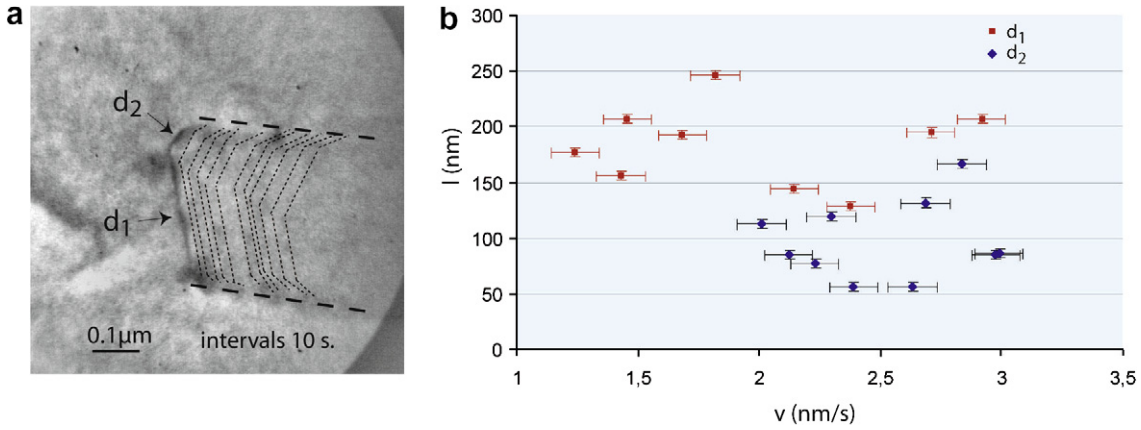

Fig. 6. In situ experiment in AlPdMn at 740 °C, showing: (a) a dislocation with straight segments d_1 and d_2 parallel to twofold directions, climbing in a fivefold plane, and (b) the corresponding instantaneous velocities of d_1 and d_2, as a function of their lengths.

This theoretical expression will be compared with experimental data in Section 4.

According to the Orowan law, the flow stress reduction observed at large strain (work-softening) may result from an increase of the density of dislocations and/or an increase of their mobility. Since observations show that the dislocation density has the opposite tendency (i.e. it decreases at increasing stress), work-softening necessarily results from an increase of the dislocation mobility [28]. A possible explanation for this effect, specific to quasicrystals, is the transposition of the easier kink-pair nucleation proposed by Takeuchi [26], to an equivalent mechanism of easier jog-pair nucleation. Another plausible explanation is an enhancement of the diffusion of vacancies, as a result of the chemical disorder produced by the storage of phason defects [29].

Average realistic values of σ^* deduced from the discussion in Section 4 are displayed in Tables 1 and 2.

2.3. The internal stress σ_i

As in crystals, an internal stress σ_i develops after a few percent of deformation. On account of Eq. (5), the steady-state stress can now be expressed as (Fig. 1c)

$$\sigma_{ss} = 2(\sigma_1^* + \sigma_{ph} + \sigma_i) \tag{11}$$

Note that the internal stress and the phason stress are both involved twice in this expression. The internal stress is given by the Taylor law $\sigma_i = \alpha\mu b\sqrt{\rho}$, where α ranges between 0.2 and 0.5, and the dislocation density is either $\rho = \rho_1 + \rho_2 = 2\rho_1$ (case of interpenetrating dislocation families) or $\rho = \rho_1 = \rho_2$ (case of two separated dislocation families). In contrast with crystals deforming by glide at low temperature, all dislocations are a priori mobile, whether they contribute to plastic deformation (family 1) or to decrease the chemical stress (family 2). This conclusion is supported by post-mortem observations showing

Table 1
Determination of the stress-dependence of the climb velocity, m, and jog-height, h, from data in the work-hardening stage

T (°C)	762 Brunner et al. [22]	750 Ledig et al. [17]	700 Ledig et al. [17]	600 Ledig et al. [17]	500 Ledig et al. [17]
σ_{el} (MPa)	150–200	200	300	650	800
$\sigma_1^* = \sigma_{el} - \sigma_{ph}$ (MPa)	120–170	170	270	630	770
r_{wh} (MPa)	55	25	40	60	90
$m_{wh} = \frac{\sigma_1^*}{r_{wh}}$	2.2–3.1	6.8	6.7	10.5	8.6
$\frac{h}{b}$	2.1	4.7	3.8	3.8	2.8

Table 2
Determination of the stress-dependence of the climb velocity, m, and jog-height, h, from data in the steady-state stage

T (°C)	762 Brunner et al. [22]	750 Ledig et al. [17]	700 Ledig et al. [17]	600 Ledig et al. [17]	500 Ledig et al. [17]
σ_{ss} (MPa)	340 (UYP)	300	500	1000	1600 (σ_{max})
σ_i (MPa)	~40	45	60	90	70
$\sigma_1^* = \frac{\sigma_{ss}}{2} - \sigma_i - \sigma_{ph}$ (MPa)	100	75	160	380	700
r_{ss} (MPa)	120	70	100	130	
$m_{ss} = \frac{2\sigma_1^*}{r_{ss}}$	1.7	2.1	3.2	5.8	
$\frac{h}{b}$	1.4	2	2.4	2.8	

The maximum stress has been used instead of the steady-state stress at 500 °C.

three-dimensional dislocation networks instead of pile-ups of climbing dislocations against dipoles [32]. In addition, the density of sessile dipoles is rather low, although they have been sometimes observed as a result of a difficult annihilation by glide [30,31], and dipole hardening appears to be negligible because global softening is observed instead of hardening.

The internal stress tends to recover by dislocation annihilation, either during the course of plastic deformation, on account of strain-softening, or during annealing [28]. Orders-of-magnitude estimates will be used to derive realistic values of σ^* in Section 4.

2.4. The phason stress σ_{ph}

At low temperatures, dislocations trail phason walls of surface energy γ, which, like stacking faults in crystals, create a back stress $\sigma_{\mathrm{ph}} = \gamma/b_{\|}$. This stress is sometimes considered to be high [34], thus accounting for the high flow stress at low temperature. Measurements deduced from the "dissociation width" of dislocations by Mompiou et al. [8], however, showed that σ_{ph} is fairly low, of the order of 30 MPa, and thus negligible at low temperature. Such a low value is expected only in case of climb, for which, contrary to glide [33], the internal tiling remains coherent behind the dislocation, with no empty space or overlap in the trace of motion, according to Gratias et al. [35].

At high-temperature, phason walls vanish rapidly in the wake of moving dislocations. The length of the phason wall trailed by a dislocation moving at the velocity v is $\lambda = vt$, where t is the time after which the phason wall has disappeared by phason dispersion. A dislocation can be considered to move in the perfect state, namely to be free of any back stress σ_{ph}, if λ is smaller than one interatomic distance. At $T \geqslant 800\ ^\circ\mathrm{C}$, this occurs for $v < 50\ \mathrm{nm\ s^{-1}}$, namely $\dot{\varepsilon} \leqslant 10^{-4}\ \mathrm{s^{-1}}$, according to Feuerbacher and Caillard [36]. This shows that almost all dislocation movements below 800 °C involve the creation of a small element of phason wall, which costs some energy. All dislocations are thus subjected to the same back stress $\sigma_{\mathrm{ph}} \approx 30$ MPa, at least below 800 °C.

3. Relaxation tests and apparent stress–strain rate sensitivity

Relaxation tests in materials deforming by climb must be analyzed considering the specific properties of the chemical stress discussed in Section 2.1. The relaxation curves and the corresponding apparent stress–strain rate sensitivities are described first in the steady-state regime and then close to the elastic limit.

During a relaxation, the total stress $\sigma = \sigma_1^* + \sigma_{\mathrm{i}} + \sigma_{\mathrm{ph}} + \sigma_{\mathrm{ch}}$ decreases according to the classical relation

$$\dot{\sigma} = -M\dot{\varepsilon}$$

where M is the elastic modulus of specimen and machine, and $\dot{\varepsilon} = \rho_1 b v_1(\sigma_1^*)$.

Assuming a power-law velocity–stress dependence, $v_1(\sigma_1^*) = A\sigma_1^{*m}$, the relaxation law becomes

$$\dot{\sigma} = -M\rho_1 bA\sigma_1^{*m} \tag{12}$$

The experimental strain-rate sensitivity, r_{exp}, is given by

$$\frac{1}{r_{\mathrm{exp}}} = \frac{\mathrm{d}\ln\dot{\varepsilon}}{\mathrm{d}\sigma} = \frac{\mathrm{d}}{\mathrm{d}\sigma}\ln -\dot{\sigma}$$

namely

$$\frac{1}{r_{\mathrm{exp}}} = m\frac{\mathrm{d}}{\mathrm{d}\sigma}\ln\sigma_1^* = m\frac{\mathrm{d}\sigma_1^*}{\mathrm{d}\sigma}\frac{1}{\sigma_1^*} \tag{13}$$

It depends on the ratio $\frac{\mathrm{d}\sigma_1^*}{\mathrm{d}\sigma}$ which, assuming that σ_{i} remains constant during the relaxation test, depends on the variation of the chemical stress σ_{ch}.

As already discussed in Section 2.1, the effective climb stress for the second system, σ_2^*, is part of the chemical stress, according to $\sigma_2^* = \sigma_{\mathrm{ch}} - \sigma_{\mathrm{i}} - \sigma_{\mathrm{ph}}$ (Fig. 1c). It tends to increase according to

$$\dot{\sigma}_2^{*+} = \theta_{\mathrm{ch}}\dot{\varepsilon} = \theta_{\mathrm{ch}}\rho_1 bA\sigma_1^{*m}$$

It also tends to decrease as a result of vacancy emission from the second system. Since this second system has the same kinetics as the first one, this trend can be expressed as

$$\dot{\sigma}_2^{*-} = \theta_{\mathrm{ch}}\rho_2 bA\sigma_2^{*m}$$

Taking $\rho_1 = \rho_2$, its total variation is thus:

$$\dot{\sigma}_2^* = \theta_{\mathrm{ch}}\rho_1 bA(\sigma_1^{*m} - \sigma_2^{*m}) \tag{14}$$

3.1. Relaxations in steady-state

The different stages of the relaxation are described schematically in Fig. 7. Assuming that $\sigma_{\mathrm{ch}} = \sigma/2$ at the beginning of the relaxation, we have $\sigma_2^* = \sigma_1^*$ (Fig. 1) which, according to Eq. (14), yields $\dot{\sigma}_2^* = 0$. The whole decrease of stress is thus supported by σ_1^*, whence $\frac{\mathrm{d}\sigma_1^*}{\mathrm{d}\sigma} = 1$, and, using Eq. (13)

$$\frac{1}{r_{\mathrm{ss}}} = \frac{m}{\sigma_1^*} \tag{15}$$

This stage extends till σ_1^* remains close to σ_2^* (full line over $t < t_{\mathrm{trans}}$ in Fig. 7).

To analyze the subsequent stages of the relaxation, it is necessary to determine the relative evolution of σ_1^* and σ_2^*. Since the relaxation is entirely supported by σ_1^*, this stress rapidly decreases to below σ_2^*. Then, Eq. (14) yields $\dot{\sigma}_2^* < 0$, which means that σ_2^* decreases in turn more and more rapidly. This transition is represented in dotted lines in Fig. 7.

The system evolves to a second stage when σ_2^* decreases at a constant rate, which, according to Eq. (14), is realized as soon as $\sigma_1^{*m} - \sigma_2^{*m}$ is constant. Assuming that $\sigma_2^* - \sigma_1^* \ll \sigma_1^*$, which is valid at the beginning of the relaxation, this condition reduces to $\sigma_2^* - \sigma_1^* = \text{constant}$, which implies that σ_1^* and σ_2^* decrease at the same rate, namely that $\dot{\sigma}_2^* - \dot{\sigma}_1^* = 0$. Assuming that $\dot{\sigma} = \dot{\sigma}_1^* + \dot{\sigma}_2^*$ (i.e. $\sigma_i \approx$

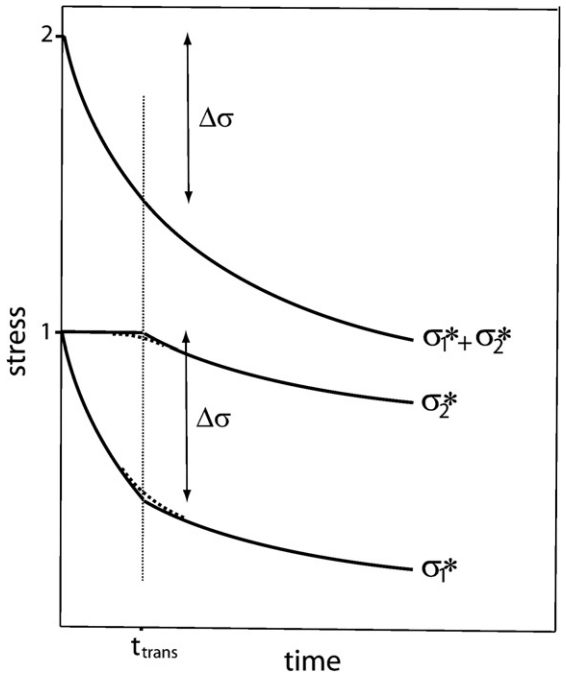

Fig. 7. Schematic description of a relaxation test in the steady-state regime (see text).

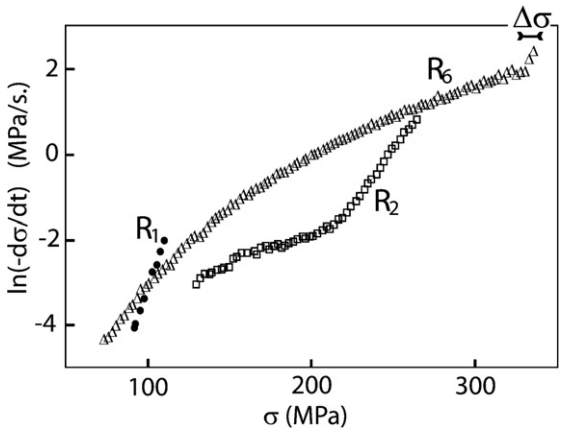

Fig. 8. Relaxation curves in the hardening stage (R_1 and R_2) and in the steady-state regime (R_6), from Ledig et al. [17]. The stress decrement $\Delta\sigma$ corresponds to that shown in Fig. 6.

constant), the latter condition is equivalent to $2\dot{\sigma}_2^* - \dot{\sigma} = 0$, which, using Eqs. (12) and (14), is verified for

$$\sigma_1^* = \sigma_2^*\left(1 + \frac{M}{2\theta_{ch}}\right)^{-1/m} \approx \sigma_2^*\left(1 - \frac{M}{2m\theta_{ch}}\right)$$

namely

$$\Delta\sigma = \sigma_2^* - \sigma_1^* = \sigma_1^*\left(\frac{M}{2m\theta_{ch}}\right) \tag{16}$$

In this second relaxation stage (full line over $t > t_{trans}$ in Fig. 7), the relation $\dot{\sigma}_2^* = \dot{\sigma}_1^*$ implies that $\dot{\sigma}_1^* = \dot{\sigma}/2$, namely $\frac{d\sigma_1^*}{d\sigma} = \frac{1}{2}$. Using Eq. (13), the apparent strain-rate sensitivity is accordingly

$$\frac{1}{r_{ss}} = \frac{m}{2\sigma_1^*} \tag{17}$$

namely twice lower than in the first period (compare with Eq. (15)).

Such a behavior has been actually observed in the experiments of Ledig et al. [17], e.g. in the relaxation R6 at 760 °C shown in Fig. 8. In this case, the decrease of stress before the transition has the right order of magnitude given by Eq. (16), namely:

$$\Delta\sigma \approx \frac{\sigma_1^*}{6} \approx 15 \text{ to } 25 \text{ MPa}$$

according to Tables 1 and 2 (see Section 4).

3.2. Relaxations in the hardening stage

At the very beginning of plastic deformation, the chemical stress is still low ($\sigma_2^* \approx 0$), and the second system is not yet activated. Eq. (14) then reduces to $\dot{\sigma}_2^* = \theta_{ch} bA(\rho_1 \sigma_1^{*m})$, which, using Eq. (12), yields:

$$\dot{\sigma}_1^* = \dot{\sigma} - \dot{\sigma}_2^* = -\rho_1 bA(M + \theta_{ch})\sigma_1^{*m}$$

$$\frac{d\sigma_1^*}{d\sigma} = \frac{\dot{\sigma}_1^*}{\dot{\sigma}} = 1 + \frac{\theta_{ch}}{M}$$

and

$$\frac{1}{r_{wh}} = \frac{m}{\sigma_1^*}\left(1 + \frac{\theta_{ch}}{M}\right)$$

In this domain, Ledig et al. corrected the apparent strain-rate sensitivity from the hardening factor $1 + \frac{\theta_{ch}}{M}$, whence

$$\frac{1}{r_{wh}^{(corr)}} = \frac{m}{\sigma_1^*} \tag{18}$$

as in the first stage of relaxations in the steady-state regime (Eq. (15)).

The corrected strain-rate sensitivity in the hardening stage is thus twice the strain-rate sensitivity in the second part of the relaxation in the steady-state regime (Eq. (17)). This ratio of two has actually been measured by Ledig et al. [17], as shown in Fig. 9.

When relaxation tests are performed after some amount of strain-hardening, the chemical stress σ_2^* cannot be neglected anymore. In a first step, as long as $\sigma_1^* > \sigma_2^*$, the relaxation takes place as above (Eq. (18)). Then, when σ_1^* has decreased to below σ_2^*, both stresses relax at the same rate and Eq. (17) holds. There is thus the same two-steps relaxation as in Section 3.1, although the transition occurs after a larger decrease of stress. Such behavior is observed in the relaxation curve R2 of Fig. 8.

4. The true stress-velocity dependence of climbing dislocations

The exponent m of the effective stress-velocity dependence can be determined using Eqs. (15), (17), or (18),

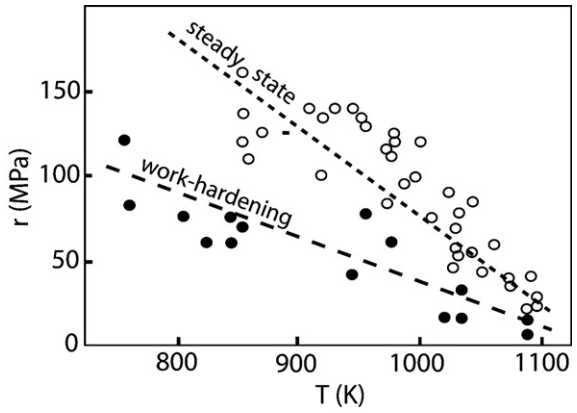

Fig. 9. Experimental values of the strain-rate sensitivity, by Ledig et al. [17]. Note the ratio of 2 between values measured in the work-hardening and steady-state stages.

provided σ_1^* is known. This has been done using data of Ledig et al. [17] and Brunner et al. [22]. The effective stress σ_1^* can be deduced from Eq. (6), where $\sigma_{ph} \approx 30$ MPa (Table 1). This value is a priori fairly relevant, because σ_{el} and σ_{ph} have been measured with a sufficiently high degree of accuracy. The effective stress can alternatively be deduced from Eqs. (7) or (11), where σ_{ph} is still of the order of 30 MPa, and σ_i is the internal stress (Table 2). The upper limit of σ_i has been estimated by Ledig et al. using the Taylor law $\sigma_i = \alpha\mu b\sqrt{\rho_1 + \rho_2}$, with $\alpha = 1$. The lower coefficient $\alpha = 0.35$ has been used here, to obtain a more reasonable estimate of σ_i. This determination is less precise than the first one, on account of the uncertainty on σ_i. The values of σ_1^* deduced from the steady-state stress are lower than those deduced from the elastic limit, especially at high-temperature. This can be attributed to strain-softening and/or to an over-estimation of the internal stress. The resulting values of m are also lower in Table 2, for the same reasons.

Tables 1 and 2 show that m increases with increasing stress and decreasing temperature, from 2.4 ± 0.6 at 762 °C to 8 ± 2 at 500–600 °C. Note that the accuracy of this determination increases with decreasing temperature.

These values of σ_1^* can now be inserted in Eq. (10), to obtain an experimental order-of-magnitude of the jog-height, h. Tables 1 and 2 show that h ranges between 1.4 $b_{\|}$ and 4.7 $b_{\|}$, the most likely value $h = 3\ b_{\|}$ corresponding to $h \sim 1$ nm, with $b_{\|} \sim 0.3$ nm. This corresponds to a Peierls mechanism (adapted to a climb process) at the scale of the cluster structure, for which the distance between Peierls valleys corresponds to the average distance between cluster rows. Note that Messerschmidt et al. [37] postulated the same value $h \sim 1$ nm, in the case of a glide mechanism.

Peierls valleys are expected to correspond to minimum values of the dislocation core energy, the origin of which is still unknown. Note that the concept of Peierls valleys in climb is relevant only when h is larger than the distance between adjacent dense rows, in such a way that several intermediate dislocation positions can be defined between them (P. Beauchamps, private communication).

5. Activation energy

According to Eq. (8a), the activation energy of plastic deformation is expected to be close to the self-diffusion energy of vacancies $U_{sd}^{(v)}$, at high stresses, and to increase to $U_{sd}^{(v)} + U_j$, as the stress decreases to zero, U_j being the energy of an isolated jog. As in ordered alloys, $U_{sd}^{(v)}$ should be related to an effective diffusion coefficient which is a weight average of the diffusion coefficients of the different constituents. Since Mn and Pd diffuse much more slowly than Al, the enthalpy of diffusion should be close to that of Mn or Pd, namely of the order of 1.7 eV [19].

Experimental values are very scattered, and entropy terms difficult to estimate. In spite of these difficulties, activation energies corrected from the variation of the shear modulus with temperature by Messerschmidt et al. [38], appear to be in a fair agreement with the above estimates. Indeed, Fig. 10 yields $\Delta G \approx 1.8$ eV $\approx U_{sd}^{(v)}$, at high stress, and the increase of ΔG extrapolated to zero stress corresponds to $U_j \approx 2$ eV, a plausible value when compared to the rough estimate given by Friedel [39] $\left(U_j \approx \frac{1}{10}\mu b^2 h \approx 2.5\ \text{eV}\right)$.

6. Discussion and consequences for crystals

The identification of chemical stresses has been possible because experiments of Ledig et al. have been carried out in a single-grained material. The same procedure in poly-grained AlPdMn would certainly yield less clear results, for two reasons: (i) chemical hardening at yield would be screened by the variable onset of plasticity of different grains (J. Bonneville, private communication), and (ii) grain boundaries may be additional sources or sinks of vacancies decreasing the chemical stress.

Up to now, climb was considered as a recovery mechanism rather than as a plasticity mechanism. This analysis

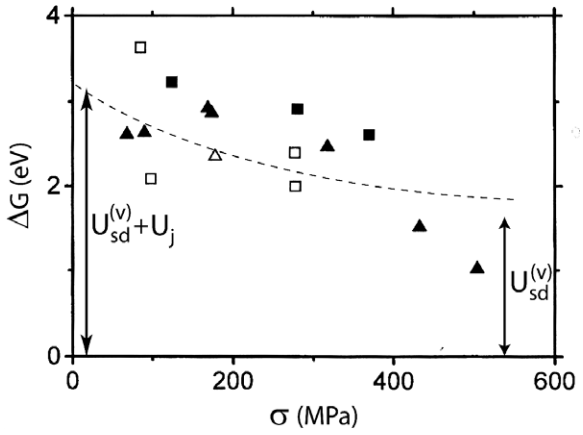

Fig. 10. Interpretation of the experimental values of activation energy measured by Messerschmidt et al. [38], in the frame of the climb model.

shows that plasticity controlled by pure climb does exist, at least above $0.65T_m$ (T_m being the absolute melting temperature), provided the stress is high enough.

In crystals, the same chemical stress and climb process should be observed as well, except for the absence of phason stress and strain-softening, under specific conditions making climb competitive with glide. As a matter of fact, the high stress level necessary to activate fast dislocation-climb cannot be reached under normal conditions, because dislocation glide is usually an easier and faster process. As mentioned in the introduction, strong evidences of various dislocation families moving by climb and exchanging vacancies have been obtained when glide is inhibited, e.g. in hcp beryllium and magnesium strained along their c-direction, and in superalloys where glide is blocked by the large γ' precipitates [2–5]. The existence of chemical forces has been postulated accordingly, but neither verified experimentally, nor explicitly included into corresponding models. In addition, several activation parameters measured in Mg have not been explained satisfactorily by these models, e.g. the stress dependence of the dislocation velocity, m, larger than unity, and the activation energy, larger than the self-diffusion energy [3]. We thus suggest that our model could be tentatively used to re-analyze these different situations.

7. Conclusions

We have proposed a model which fully accounts for several unexplained aspects of the mechanical properties of icosahedral AlPdMn, measured by Ledig et al. [17]. This model, which is based on our post-mortem and in situ TEM observations of pure climb dislocation motion, provides the first direct evidence of the chemical force induced by an out-of-equilibrium vacancy concentration. It relies on the following properties which can be considered as the signature of pure climb plasticity:

- a high strain-hardening at yield, due to a strong decrease of the concentration of vacancies consumed by climbing dislocations;
- a steady-state flow stress twice higher than the elastic limit, which is accounted for by the equilibrium value of the chemical stress;
- two-stages relaxation curves defining strain-rate sensitivities in a ratio of 2, which are a direct consequence of the complex relaxation of the chemical stress.

The true stress-dependence of the dislocation-climb velocity, which has been determined accordingly, is different from the linear dependence given by classical models valid at low stress and high temperature. It is, however, in fair agreement with the model of Hirth and Lothe, which describes the nucleation of jog pairs on straight dislocation segments observed in TEM. The best fit is obtained for a jog-height of about 1 nm, i.e. of the order of the average distance between cluster rows.

These conclusions may be transposed to crystals deformed under specific conditions favouring pure climb deformation.

Appendix

We establish here the relation $\rho_{1ss} = \rho_{2ss}$ which has been used to derive Eq. (5). The dislocation density ρ_1 involves all Burgers vectors almost parallel to the compression axis (corresponding Schmid factor close to unity), whereas ρ_2 involves all Burgers vectors almost perpendicular to the compression axis (corresponding Schmid factor with respect to the chemical stress close to unity). These dislocations are assumed to have N_1 and N_2 different Burgers vectors, respectively. With a fivefold compression axis, we consider $N_1 = 6$ (one Burgers vector along the compression axis, $b = 0.456$ nm and five ones along the twofold directions inclined at 30° from the compression axis, $b = 0.480$ nm), and $N_2 = 5$ (the five Burgers vectors with twofold directions perpendicular to the compression axis, $b = 0.480$ nm). These Burgers vectors actually correspond to those observed in Ref. [8]. Assuming that (i) all Burgers vectors have the same length, and (ii) all Schmid factors are equal to unity, each system accounts for a fraction $\dot{\varepsilon}/N_1$, or $\dot{\varepsilon}/N_2$, of the total strain rate $\dot{\varepsilon}$, which is the same for families 1 and 2 (Eq. (4)).

Dislocations multiply and annihilate until a steady-state is reached. This evolution is first described by equations already used by Guyot and Canova [40] and Feuerbacher et al. [41] (case 1). Since these equations are based on a glide process, we subsequently use other equations better adapted to climb (case 2). In each approximation, we consider situations where all dislocation systems evolve either independently or not.

Case 1: the evolution of dislocation density with time is often described by the following equation [40,41]:

$$\dot{\rho} = \frac{M}{b}\dot{\varepsilon}\sqrt{\rho} - \frac{Y}{b}\rho\dot{\varepsilon}$$

The first term describes the athermal storage of dislocations, which depends on their swept area per unit time, $\dot{\varepsilon}/b$, and on their mean free traveling distance, determined by the average dislocation spacing $\rho^{1/2}$ [42,43]. The second term, proportional to the current dislocation density, describes the annihilation of dislocations by dynamic processes. The dimensionless parameter Y/b, where Y is related to the characteristic annihilation distance, has been introduced by Kocks [42]. For a glide process, Y has been shown experimentally to follow a power law, $Y = A\dot{\varepsilon}^{-1/n}$, where n is of the order of 5 [43,44].

Independent dislocation systems: if all systems develop in different areas, we have for the two families:

$$\begin{cases} \dot{\rho}_1^j = \frac{M}{b}\frac{\dot{\varepsilon}}{N_1}\sqrt{\rho_1^j} - \frac{A}{b}\left(\frac{\dot{\varepsilon}}{N_1}\right)^{1-\frac{1}{n}}\rho_1^j \\ \dot{\rho}_2^j = \frac{M}{b}\frac{\dot{\varepsilon}}{N_2}\sqrt{\rho_2^j} - \frac{A}{b}\left(\frac{\dot{\varepsilon}}{N_2}\right)^{1-\frac{1}{n}}\rho_2^j \end{cases}$$

At the steady-state, the dislocation densities are given by $\dot{\rho}_{1,2}^{i,j} = 0$, i.e.:

$$\rho_{1ss} = N_1^{1-\frac{2}{n}}\left(\frac{M}{A}\right)^2 \dot{\varepsilon}^{2/n},$$
$$\rho_{2ss} = N_2^{1-\frac{2}{n}}\left(\frac{M}{A}\right)^2 \dot{\varepsilon}^{2/n}, \text{ and } \frac{\rho_{1ss}}{\rho_{2ss}} = \left(\frac{N_1}{N_2}\right)^{1-\frac{2}{n}} \quad (A.1)$$

Overlapping dislocation systems: if all dislocation systems develop in the same area, the dislocation mean free path is $\rho^{1/2}$, whence:

$$\begin{cases} \dot{\rho}_1^i = \frac{M}{b}\frac{\dot{\varepsilon}}{N_1}\sqrt{\rho} - \frac{A}{b}\left(\frac{\dot{\varepsilon}}{N_1}\right)^{1-\frac{1}{n}}\rho_1^i \\ \dot{\rho}_2^j = \frac{M}{b}\frac{\dot{\varepsilon}}{N_2}\sqrt{\rho} - \frac{A}{b}\left(\frac{\dot{\varepsilon}}{N_2}\right)^{1-\frac{1}{n}}\rho_2^j \end{cases}$$

This yields:

$$\rho_{1ss} = N_1^{1-\frac{1}{n}}\left(\frac{M}{A}\right)\sqrt{\rho}\dot{\varepsilon}^{1/n},$$
$$\rho_{2ss} = N_2^{1-\frac{1}{n}}\left(\frac{M}{A}\right)\sqrt{\rho}\dot{\varepsilon}^{1/n}, \text{ and } \frac{\rho_{1ss}}{\rho_{2ss}} = \left(\frac{N_1}{N_2}\right)^{1-\frac{1}{n}} \quad (A.2)$$

Case 2: In pure climb plasticity, there is no dislocation storage, as a result dislocation multiplication is only proportional to $\dot{\varepsilon}$. The annihilation rate depends on the current dislocation density ρ and on the annihilation speed. The latter is driven by the internal stress (static recovery) and proportional to $\sigma_{int}^m \propto \rho^{m/2}$. This can be expressed as $\dot{\rho} = B\dot{\varepsilon} - C\rho^{1+\frac{m}{2}}$, where B and C are constants.

In the case of N_1 and N_2 independent families, this yields:

$$\begin{cases} \dot{\rho}_1^i = B\frac{\dot{\varepsilon}}{N_1} - C(\rho_1^i)^{1+\frac{m}{2}} \\ \dot{\rho}_2^j = B\frac{\dot{\varepsilon}}{N_2} - C(\rho_1^j)^{1+\frac{m}{2}} \end{cases}$$

At the steady-state this leads to

$$\rho_{1ss} = N_1\left(\frac{B}{C}\right)^{\frac{2}{m+2}}\left(\frac{\dot{\varepsilon}}{N_1}\right)^{\frac{2}{m+2}},$$
$$\rho_{2ss} = N_2\left(\frac{B}{C}\right)^{\frac{2}{m+2}}\left(\frac{\dot{\varepsilon}}{N_2}\right)^{\frac{2}{m+2}}, \text{ and } \frac{\rho_{1ss}}{\rho_{2ss}} = \left(\frac{N_1}{N_2}\right)^{\frac{m}{m+2}} \quad (A.3)$$

In the case of overlapping families, we have

$$\begin{cases} \dot{\rho}_1^i = B\frac{\dot{\varepsilon}}{N_1} - C\rho_1^i\rho^{m/2} \\ \dot{\rho}_2^j = B\frac{\dot{\varepsilon}}{N_2} - C\rho_2^i\rho^{m/2} \end{cases}$$

At the steady-state this yields:

$$\rho_{1ss} = \frac{B}{C}\dot{\varepsilon}\rho^{-m/2}, \quad \rho_{2ss} = \frac{B}{C}\dot{\varepsilon}\rho^{-m/2}, \text{ and } \frac{\rho_{1ss}}{\rho_{2ss}} = 1 \quad (A.4)$$

Considering that $N_1 \approx N_2$, $n \approx 5$, and $2 < m < 10$, Eqs. (A.1)–(A.4) yield $\rho_{1ss} \approx \rho_{2ss}$. Many others calculations could be made, which would yield similar results.

References

[1] Nabarro FRN. Phil Mag 1967;16:231.
[2] Le Hazif R, Antolin J, Dupouy JM. Trans JIM 1968;9(Suppl.):247.
[3] Edelin G, Poirier JP. Phil Mag 1973;28:1203–11.
[4] Epishin A, Link T. Phil Mag 2004;84:1979.
[5] Caillard D. Mater Sci Eng A. submitted for publication.
[6] Caillard D, Martin JL. In: Cahn RW, editor. Thermally activated mechanisms in crystal plasticity. Pergamon materials series. Pergamon; 2003.
[7] Caillard D, Vanderschaeve G, Bresson L, Gratias D. Phil Mag 2000;80:237.
[8] Mompiou F, Bresson L, Cordier P, Caillard D. Phil Mag 2003;83:3133.
[9] Caillard D, Mompiou F, Bresson L, Gratias D. Scripta Mater 2003;49:11.
[10] Mompiou F, Caillard D. Phil Mag 2004;84:555.
[11] Mompiou F, Caillard D, Feuerbacher M. Phil Mag 2004;84:2777.
[12] Mompiou F, Caillard D. Mater Sci Eng A 2005;400–401:283.
[13] Messerschmidt U, Bartsch M. Scripta Mater 2003;49:33.
[14] Bonneville J, Caillard D, Guyot P, Dislocations in solids, vol. 14, in press.
[15] Socolar JES, Lubensky TC, Steinhardt PJ. Phys Rev B 1986;34:3345–60.
[16] Wollgarten M, Zhang Z, Urban K. Phil Mag Lett 1992;65(1):1–6.
[17] Ledig L, Bartsch M, Messerschmidt U. Mater Sci Eng A 2006;429:79.
[18] Sato K, Takahashi Y, Uchiyama H, Kanazawa I, Tamura R, Kimura K, et al. Phys Rev B 1999;59:6712.
[19] Galler R, Mehrer H. Mater Sci Eng A 2000;294–296:693.
[20] Messerschmidt U, Ledig L, Bartsch M. J Non Crystall Solids 2004;334–335:436.
[21] Cahn JW, Shechtman D, Gratias D. J Mater Res 1989;1:13.
[22] Brunner D, Plachke D, Carstanjen HD. Mater Sci Eng A 2000;294–296:773.
[23] Geyer B, Bartsch M, Feuerbacher M, Urban K, Messerschmidt U. Phil Mag A 2000;80:1151.
[24] Hirth JP, Lothe J. Theory of dislocations. 2nd ed. New York: Mc Graw Hill; 1968.
[25] Caillard D, Martin JL. Int Mater Rev 2005;50:366.
[26] Takeuchi S. Mater Sci Eng A 2005;400–401:306.
[27] Mompiou F. Thèse, Toulouse: Université Paul Sabatier; 2004.
[28] Schall P, Feuerbacher M, Bartsch M, Messerschmidt U, Urban K. Phil Mag Lett 1999;79:785.
[29] Franz V, Feuerbacher M, Wollgarten M, Urban K. Phil Mag Lett 1999;79:333.
[30] Mompiou F, Caillard D. Phil Mag Lett 2004;84:555.
[31] Texier M, Bonneville J, Proult A, Rabier J, Thilly L. MRS Symp Proc 1999;805:LL5-3-1.
[32] Messerschmidt U, Petrukhov BV, Bartsch M, Dietzsch CH, Geyer B, Hausler D, et al. Mater Res Eng A 2001;319–321:107.
[33] Takeuchi S. MRS Symp Proc 1999;553:283.
[34] Mikulla R, Roth J, Trebin HR. Phil Mag B 1995;5:981.
[35] Gratias D, Beauchesne JT, Mompiou F, Caillard D. Phil Mag 2006;86:4139.
[36] Feuerbacher M, Caillard D. Acta Mater 2006;54:3233.
[37] Messerschmidt U, Bartsch M, Feuerbacher M, Geyer B, Urban K. Phil Mag A 1999;79:2123.
[38] Messerschmidt U, Bartsch M, Geyer B, Feuerbacher M, Urban K. Phil Mag A 2000;80:1165.
[39] Friedel J. Dislocations. Oxford: Pergamon Press; 1964.
[40] Guyot P, Canova G. Phil Mag A 1999;79(11):2815.
[41] Feuerbacher M, Schall P, Estrin Y, Brechet Y. Phil Mag Lett 2001;81(7):473.
[42] Kocks UF. J Eng Matter Tech (ASME H) 1976;98:76.
[43] Estrin Y, Mecking H. Acta Metall 1984;32(1):57.
[44] Mecking H, Kocks UF. Acta Metall 1981;29:1865.